Quaternary blends of Portland cement, metakaolin, biomass ash, and granite powder for production of self-compacting concrete

Gemma Rojo-López[a], Sandra Nunes[b], Belén González-Fonteboa[c], Fernando Martínez-Abella[d]

[a]**PhD Student at the School of Civil Engineering**. Department of Civil Engineering, University of A Coruña. E.T.S.I. Caminos, Canales, Puertos, Campus Elviña s/n, 15071, La Coruña, Spain. **E-mail**: gemma.rojo@udc.es. **Telephone number**: (+34) 881016308.

[b]**Assistant Professor,** CONSTRUCT-LABEST, Faculty of Engineering (FEUP), University of Porto, Rua Dr. Roberto Frias-4200-465 Porto, Portugal. **E-mail**: snunes@fe.up.pt. **Telephone number**: (+351) 225082121.

[c]**Associate Professor at the School of Civil Engineering**. Department of Civil Engineering, University of A Coruña. E.T.S.I. Caminos, Canales, Puertos, Campus Elviña s/n, 15071, La Coruña, Spain. **E-mail**: bfonteboa@udc.es **Telephone number**: (+34) 881011442.

[d]**Professor at the School of Civil Engineering**. Department of Civil Engineering, University of A Coruña. E.T.S.I. Caminos, Canales, Puertos, Campus Elviña s/n, 15071, La Coruña, Spain. **E-mail**: fmartinez@udc.es. **Telephone number**: (+34) 881011443.

Abstract

Given the rising societal pressure towards sustainable waste management and resource efficiency, in a more circular economy, an increased use and diversification of supplementary cementitious materials (SCM) will be necessary to achieve the CO_2 mitigation goals. The current study addresses the development of self-compacting concrete, replacing part of the cement (the primary source of CO_2 emissions) by metakaolin and wastes derived from two industrial sectors operating in the "Galicia–North of Portugal Euroregion": wood manufacturing and natural stone quarrying. A study was carried out at the mortar level to investigate the effect of the mix design variables on several engineering properties of the self-compacting concrete. Statistically designed experiments reveal that an increase in water/powder volume ratio has a dominant effect on the fresh state properties, whereas the water/cement weight ratio has a dominant effect on the hardened state properties. A like-for-like comparison of the proposed quaternary blends and previously studied binary/ternary blends indicates that these mixtures exhibit improved self-compacting ability, greater compressive strength, and can offer interesting opportunities to reduce the unit cost and environmental impact of self-compacting concrete per m^3. Four different mortar mixtures were optimised to achieve excellent self-compacting ability

This is an accepted version of the following published document: https://doi.org/10.1016/j.jclepro.2020.121666

yet with distinct compressive strength levels at 28 days (65, 70, 75, and 80 MPa). A single measure of the material efficiency is proposed herein to reflect the engineering properties improvement (workability, compressive strength, and durability) over its economic (unit cost) and environmental impact.

Keywords: waste minimisation; statistical factorial design; metakaolin; biomass ash; granite powder; material efficiency

List of abbreviations

CCD	Central composite design
Fi	Factorial points
Ci	Central points
CCi	Axial points
Vw/Vp	Water to powder volume ratio
w/c	Water to cement weight ratio
Sp/p	Superplasticizer to powder weight ratio
ash/c	Biomass ash to cement weight ratio
Vgp/Vp	Granite powder to powder volume ratio
Vs/Vm	Sand to mortar volume ratio
mk/c	Metakaolin to cement weight ratio
Dflow	Spread diameter
Tfunnel	Time to flow through the funnel
fcm_28d	Compressive strength at 28 days
Resist_id	Electrical resistivity at i days
Por_28d	Porosity accessible to water at 28 days
Carb_6m	Carbonation depth after 6 months of exposure inside the carbonation chamber
GWP	Global warming potential
ME	Material efficiency
Ref	Reference value for several factors
wi	Partial weights to each engineering property
y	Response variable in model
xi and xj	Design variables in model
β0, βi, βii, βij	Tuning parameters in models
ε	Residual error in models
ρc	Cement density

ρmk	Metakaolin density
ρBA	Biomass ash density
ρw	Water density
d	Distance to the centre of the CCD plan
OP_i	Optimum mixtures

1 INTRODUCTION

The construction industry has an important role in terms of environmental respect and sustainable development, with cement production being the main process influencing this issue. In fact, the CO_2 emissions associated with the production of 1 ton of cement are approximately 1 ton of CO_2. Therefore, construction has a challenge to initiate critical steps toward sustainability. The United Nations Environment Programme (UNEP) (Scrivener et al., 2016) summarises the key conclusions of an analysis on low-CO_2, eco-efficient cement-based materials. This programme states that there are two different possibilities to produce sustainable concretes and mortars: “increased use of low-CO_2 supplements as partial replacements for Portland cement clinker” and “more efficient use of Portland cement clinker in mortars and concretes”. The evolution of recent scientific publications reflects it is clear that the scientific community is following these recommendations.

Fig. 1. displays the evolution (from 2000 to 2018) of journal papers that include the following words “supplementary cementitious materials” and “concrete” in the following items: “Article title”, “Abstract”, and “Keywords”. The growing interest in issues related to concrete sustainability is clear (blue line).

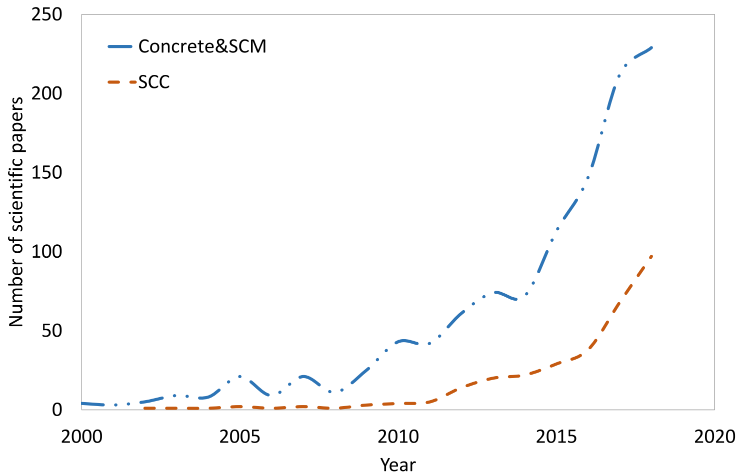

Fig. 1. Evolution of number of papers published on concrete sustainability (Source: Query on Scopus data; date: Nov, 2019)

A new search within the previous results, identifying those journal papers that address "self-compacting concrete" (SCC) (orange line in Fig. 1.) also indicates a significant increasing trend. SCC is a concrete family that differs from conventional vibrated concrete only when observed at fresh state (Khayat and De Schutter, 2014). Its main characteristic is the ability to fill the formwork and consolidate under its own weight without any compaction. Despite the larger consumption of powder materials (including cement) and chemical admixtures, SCC, due to the absence of the need of vibration, better physical and mechanical properties and greater durability, can be a superior construction material in terms of environmental impact in comparison to conventional vibrated concrete. In the short-medium term, reducing cement consumption by using supplementary cementitious materials (pozzolanic or non-pozzolanic) (de Azevedo et al., 2020; Paris et al., 2016) or by using optimized aggregate grading (Amaral et al., 2020; Esmaeilkhanian et al., 2017), and the incorporation of a wide range of recycled aggregates (González-Taboada et al., 2017) provide opportunities to further improve environmental performance of SCC. In the longer term, the use of non-Portland clinkers (Gartner and Hirao, 2015) and alkali-activated binder technologies (Shi et al., 2019) have also the potential to deliver significant reductions in CO_2 emissions of the construction sector (Scrivener et al., 2018).

Based on an analysis of 1352 SCC mixtures carried out by Desnerck et al. the most commonly used addition materials in SCC are limestone filler (41%), fly ash (35%), ground granulated blast-furnace slag (9%) and silica fume (9%) (Khayat and De Schutter, 2014). Less common addition materials but nonetheless used in some cases, are vegetable ashes (2%), metakaolin (0.7%), and other types of fillers like marble powder or granite powder (<0.5%). The amounts of high quality addition materials, such as ground granulated blast-furnace slag, fly ash and silica fume, available worldwide is relatively limited taking into account the future growing demand of cement (and concrete) and at the same time the need to further reduce CO_2 emissions (Scrivener et al., 2018). For these reasons, metakaolin has become the pozzolanic addition with an increasing application in the concrete industry. This addition costs less than silica fume and provides advantages in terms of energy consumption and CO_2 emissions, because it requires reduced manufacturing temperatures compared to cement clinker (Siddique and Klaus, 2009). Rice husk ash can also replace silica fume; however, its availability is also limited in some countries (Swaminathen, 2013). In addition to these pozzolanic additions, the use of non-pozzolanic industrial wastes as additions for SCC production is growing (Aprianti S, 2017; Mo et al., 2016). One example is limestone filler, which is abundantly available, but it can be added alone to Portland cement only in modest amounts (up to 10-15%) to avoid significant performance loss. Therefore, not only binary, but also ternary and quaternary blends of several different supplementary cementitious materials (pozzolanic and non-pozzolanic) have been investigated to produce SCC (Saleh Ahari et al., 2015; Uysal and Sumer, 2011; Vance et al., 2013; Sadek et al., 2016; Ho et al., 2002; Abd Elmoaty, 2013)

To go further with the successful strategy of reducing cement consumption in SCC it is essential to find new types and sources of powder materials. The proposed new solutions, to be adopted on a significant scale, must be abundantly available and have low cost. This cost must consider the source of the alternative material, its transportation, processing, and should consider savings through diversion from landfilling. Adding value to by-products of other industries is another positive step, given the rising awareness towards sustainable waste management and resource efficiency in a more circular economy.

1.1 Research scope and objectives

In the current study, one searched for wastes generated from local industry in the "Galicia–North of Portugal Euroregion" ('Eurorregión Galicia-Norte de Portugal (AECT) | POCTEP', n.d.), abundantly available, and that could be suitable for use in SCC. Two main industry sectors were identified: wood manufacturing and natural stone quarrying.

Wood manufacturing sector produces several types of wastes, one of them is forest biomass, generated by different operations in wood production, and in forest energy crops. This waste is understood (in energy terms) as a fuel derived from natural products and residues, and it is used for energy production by calcination. This use, recognised by EU in the Green Book (Europeas, 2000), can contribute significantly to strengthening the security of a sustainable supply. Table 1 displays the quantities of forest biomass generated in the Galicia–North Portugal Euroregion.

Table 1. Forest biomass generated in Galicia–North Portugal Euroregion (data from 2016/2017) (Enersilva, 2007)

Region	PFB (t)
Galicia	490 199
North Portugal	2 242 193

The use of biomass as a fuel requires knowledge of its properties and the characterisation and quantification of the resources to be exploited. This use reduces costs; however, it produces a significant amount of ash waste from the incineration process. The use of this waste in the construction field as a raw material offers the opportunity for not only protecting the environment, but also saving costs and natural resources. To use this biomass ash, it is important to know and control its properties as there are several factors that influence them, including the heat treatment temperature or tree species used (Cheah and Ramli, 2011).

Spain and Portugal are in the top ten and top three producers of natural stone in the world and in the European Union, respectively, (Montani, 2017). Moreover, 65% of the Spanish production is generated in Galicia; hence, the Galicia–North Portugal Euroregion has an important role in the worldwide natural stone industry. The ornamental stone industry produces a sludge waste generated during cutting and polishing operations where water is used to cool and lubricate the machines. This generated waste has environmental, health, and economical drawbacks. The waste quantities generated in the Euroregion are presented in Table 2. Research works published between 1992 and 2014, and summarised by Galetakis and Soultana (Galetakis and Soultana, 2016), indicated that ornamental stone waste (mainly from marble and granite) can be used as a cement replacement material in a wide range (between 5 and 50%). However, this use implies a deep knowledge about of its properties and possible secondary effects on the final construction material. For example, the addition of high quantities of this fine waste in concrete can influence the water demand, which has an effect on the shrinkage deformation, and mechanical and durability properties.

Table 2. Processing waste (× 10^3 t) (Montani, 2017)

Country	1994	2000	2009	2010	2011	2012	2013	2014	2015	2016
Portugal	728	942	857	877	820	818	788	798	812	785
Spain	1540	2337	1955	1998	1756	1627	1544	1612	1641	1760

The aim of the present work is to investigate the effects of replacing Portland cement by biomass ash, granite powder and metakaolin on the behaviour of SCC-mortar mixes; and to optimize the respective mixture proportions in order to achieve distinct compressive strength levels and similar self-compacting ability, thus, creating alternative quaternary binders. This study aims also to quantify the global performance of the novel quaternary binders associating not only the technical requirements (mechanical and durability properties), but also the economic and the global warming potential of concrete on a volumetric basis.

1.2 Research significance

From the preceding literature review, no work has been developed using quaternary blends of Portland cement, metakaolin, biomass ash and granite powder to produce SCC. In this paper, the Design of Experiments (DoE) approach was adopted and a Central Composite Design plan was selected that allows, with a minimum number of experiments, an understanding of the relationships between the main design variables (mix-proportion ratios) and relevant response variables (mortar properties). In addition, it offers a valid basis for developing empirical models that allow optimising the mix proportions for a given set of performance requirements. A material efficiency indicator (ME) is proposed herein as a first step towards associating environmental impact and performance requirements in SCC mix-design. This simple indicator has the potential ability to allow concrete technologists to balance the societal demand in terms of CO_2 emissions mitigation with the performance requirements and cost. By promoting the use of low-CO_2 supplementary materials, as partial replacement for Portland cement, this research contributes to: (i) fill the knowledge gap that currently exists in regard to this type of quaternary binder blends; (ii) further improve the environmental performance of SCC; (iii) mitigate solid waste disposal of in landfills; and (iv) turn two industrial wastes into a product with added-value for local construction industry.

2 MATERIAL AND METHODS

2.1 Powder materials and aggregates

Mortar mixes were prepared with a commercial Portland cement labelled as CEM I 52.5 N-SR5 (CEM). Other powder materials were used in the mixtures, namely metakaolin (MK), granite powder (GP), and biomass ash (BA). For these powder materials, the pozzolanic activity was assessed according to French standard NF P18-513 (AFNOR, 2012). Following the literature recommendations, the lower limit to be considered pozzolanic activity was 650 mg of $Ca(OH)_2$ (Pavlíková et al., 2019); hence, in this study, only metakaolin could be considered pozzolanic.

Metakaolin is a pozzolanic material that can be used in a wide range, partially replacing cement. Owing to its pozzolanic activity, it is expected to contribute to increase of the strength and durability of the mortar mixes (Matos et al., 2018). Granite powder and biomass ash are wastes of different local industries. Granite waste, in the form of sludge, is produced during the granite wet cutting and wet polishing processes. After drying, this sludge can be converted into a powder material and incorporated into the mortar mixtures with no other treatment. Biomass ash is obtained from biomass boilers and extracted by gas cleaning cyclones in the fibreboard manufacturing industry. Table 3 displays the main chemical and physical properties of cement, metakaolin, granite powder, and biomass ash.

Table 3. Main chemical and physical properties of powder materials

% by mass	CEM	MK	GP	BA
SiO_2	18.9	58.0	70.4	40.0
Al_2O_3	6.3	36.8	15.2	16.6
Fe_2O_3	2.7	1.2	2.0	5.5
CaO	59.9	0.075	1.0	10.2
K_2O	1.9	2.1	5.5	6.9
Na_2O			3.7	1.6
MgO	1.6	0.18	0.35	2.8
SO_3	3.5	0.058		2.4
LOI	4.3	0.7	1.0	2.7
Specific density (g/cm^3)	3.04	2.55	2.56	2.68
Specific surface area BET (m2/g)	1.36	4.25	8.77	0.63
Pozzolanic activity (mg of $Ca(OH)_2$)		946	48	258

The gradation of all powder materials obtained by laser diffraction is displayed in Fig. 2. The fineness of the cement is similar to the fineness of the metakaolin. The granite powder is finer than cement, whereas the biomass ash is coarser than cement. The differences between granite powder and biomass ash in terms of particles shape and size can be observed in Fig. 3. Therefore, it was decided to combine these two waste materials in this work, along with cement and metakaolin, to maximise the packing density of all the powder materials and propose novel quaternary binders.

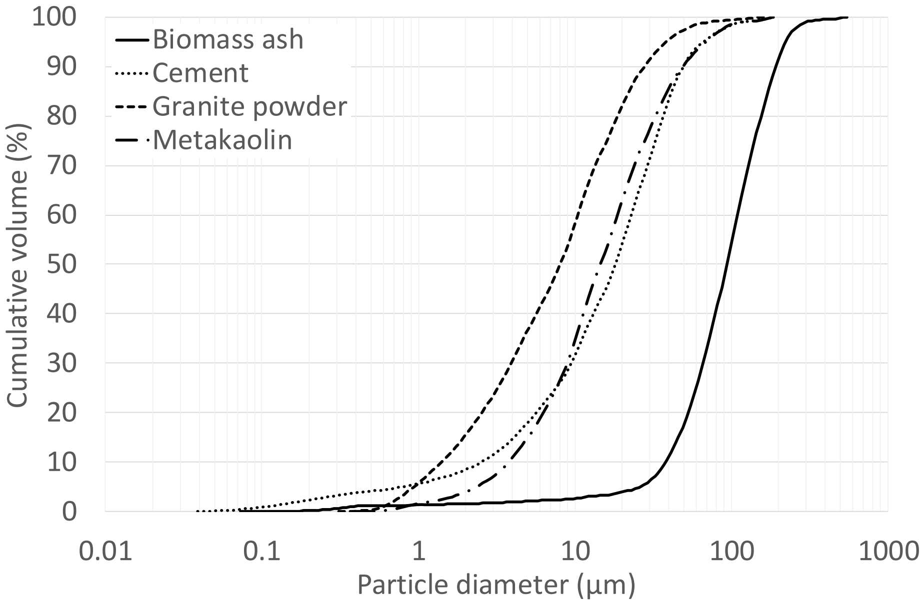

Fig. 2. Particle size distribution of powder materials

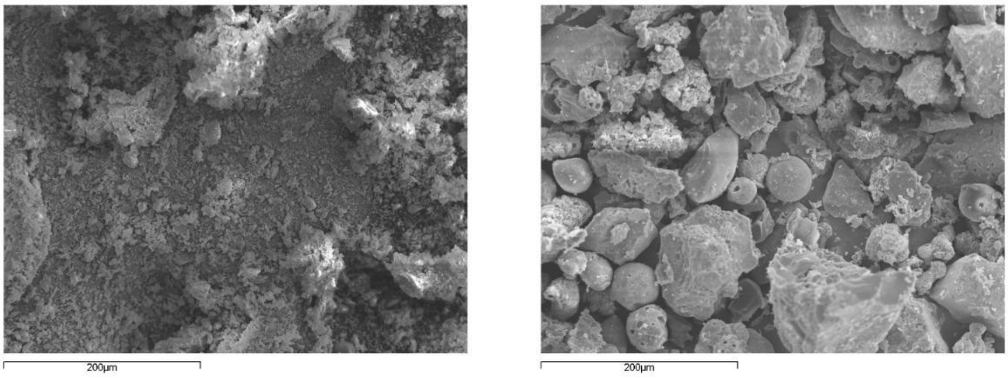

(a) (b)

Fig. 3. SEM images: (a) granite powder (b) biomass ash

Tap water and a polycarboxylate-based superplasticizer (Sp) (density of 1.05 g/cm³and 20.3% solids content) were used in this investigation. A standard sand was used conforming to EN 196-1 (AENOR, 2005). This is a natural siliceous sand with round-shaped particles with sizes ranging from 0.08 mm to 2 mm, specific gravity of 2.63, and water absorption of 0.3%, by mass.

2.2 Experimental plan

In this work, experiments were planned according to a complete factorial plan 2^4, corresponding to four factors and two levels per factor. Considering that the investigated properties were not expected to change linearly within the experimental region, eight axial points (CCi) and four central points (Ci) were added to the factorial plan, resulting in a central composite design (CCD), which allows to fit a second-order polynomial model (Montgomery, 2012). The selected independent variables were the following: water to powder volume ratio (Vw/Vp); water to cement weight ratio (w/c); SP to powder weight ratio (Sp/p); and biomass ash to cement weight ratio (ash/c). In this manner, the effects of the independent variables were evaluated at five different levels, namely -α, -1, 0, +1, and + α in terms of coded values. More information regarding the DOE approach can be found in (Montgomery, 2012). The value of α was chosen to ensure that the CCD was rotatable Eq. Eq. 1):

$$\alpha = nf^{1/4}, \qquad \textbf{Eq. 1}$$

where nf is the number of factorial points in the plan (identified as Fi in Table 5)). In the present study nf = 16, thus leading to α = 2.

The investigated levels of independent variables in terms of actual and coded values is provided in Table 4. The mixtures were proportioned with constant fine aggregate content and a metakaolin to cement weight ratio: Vs/Vm = 0.475 and mk/c = 0.20, respectively. Table 5 presents an overview of the complete CCD plan of experiments including 25 different mortar mixtures. The amount of fine aggregate was constant for all mixes and equal to 1249.25 kg/m^3.

Statistical methods in experimental design approach require that the observations (or errors) be independently distributed random variables (Montgomery, 2012). Thus, both the allocation of constituent materials and the order in which the individual runs were performed were randomly determined. The four replicate runs of central points (C_i in Table 5) were spread out in time (an exception to the randomization rule mentioned before) to get a rough check on the stability of the process during the experimental programme. In addition, a few trial runs before conducting the experimental plan were carried out to check the adequacy of the selected range of mixture parameters, to check on the measurement systems and to practice the overall experimental techniques.

Table 4. Actual and coded values of independent variables (mix-design variables)

Independent variables	-2	-1	0	1	2
Vw/Vp	0.75	0.8	0.85	0.9	0.95
w/c	0.4	0.45	0.5	0.55	0.6
Sp/p	0.015	0.0155	0.016	0.0165	0.017
ash/c	0.1	0.125	0.15	0.175	0.2

Table 5. Mixture proportions (kg/m^3)

Ref.	Vw/Vp	w/c	Sp/p	ash/c	CEM	MK	BA	GP	Water	Sp
Ci (i=1 to 4)	0	0	0	0	480.57	96.11	72.09	165.49	240.29	13.03
F1	-1	-1	-1	-1	516.52	103.30	64.57	154.42	232.44	13.00
F2	1	-1	-1	-1	550.60	110.12	68.83	69.42	247.77	12.38
F3	-1	1	-1	-1	422.62	84.52	52.83	272.47	232.44	12.90
F4	1	1	-1	-1	450.51	90.10	56.31	195.26	247.78	12.28
F5	-1	-1	1	-1	516.39	103.28	64.55	154.38	232.38	13.84
F6	1	-1	1	-1	550.47	110.10	68.81	69.40	247.71	13.18
F7	-1	1	1	-1	422.51	84.50	52.81	272.40	232.39	13.73
F8	1	1	1	-1	450.40	90.08	56.30	195.21	247.72	13.07

F9	-1	-1	-1	1	516.52	103.31	90.39	127.78	232.44	12.99
F10	1	-1	-1	1	550.60	110.12	96.36	41.03	247.77	12.37
F11	-1	1	-1	1	422.62	84.52	73.96	250.67	232.44	12.89
F12	1	1	-1	1	450.51	90.10	78.84	172.03	247.78	12.27
F13	-1	-1	1	1	516.39	103.28	90.37	127.75	232.38	13.82
F14	1	-1	1	1	550.47	110.10	96.33	41.02	247.72	13.17
F15	-1	1	1	1	422.52	84.50	73.94	250.61	232.39	13.72
F16	1	1	1	1	450.40	90.08	78.82	171.98	247.72	13.06
CC1	-2	0	0	0	448.17	89.63	67.23	251.56	224.09	13.71
CC2	2	0	0	0	509.65	101.93	76.45	88.21	254.83	12.42
CC3	0	-2	0	0	600.69	120.14	90.10	11.38	240.28	13.16
CC4	0	2	0	0	400.48	80.10	60.07	268.23	240.29	12.94
CC5	0	0	-2	0	480.68	96.14	72.10	165.53	240.34	12.22
CC6	0	0	2	0	480.45	96.09	72.07	165.45	240.23	13.84
CC7	0	0	0	-2	480.57	96.11	48.06	190.27	240.29	13.04
CC8	0	0	0	2	480.57	96.11	96.11	140.71	240.29	13.02

With the current experimental plan, a significant portion of the powder materials consisted of waste materials and metakaolin, as illustrated in Fig. 4. The volumes of cement, metakaolin, granite powder, and biomass ash, with reference to the total volume of the fines, ranged from 47% to 70%, 11% to 17%, 1% to 34%, and 6% to 13%, respectively.

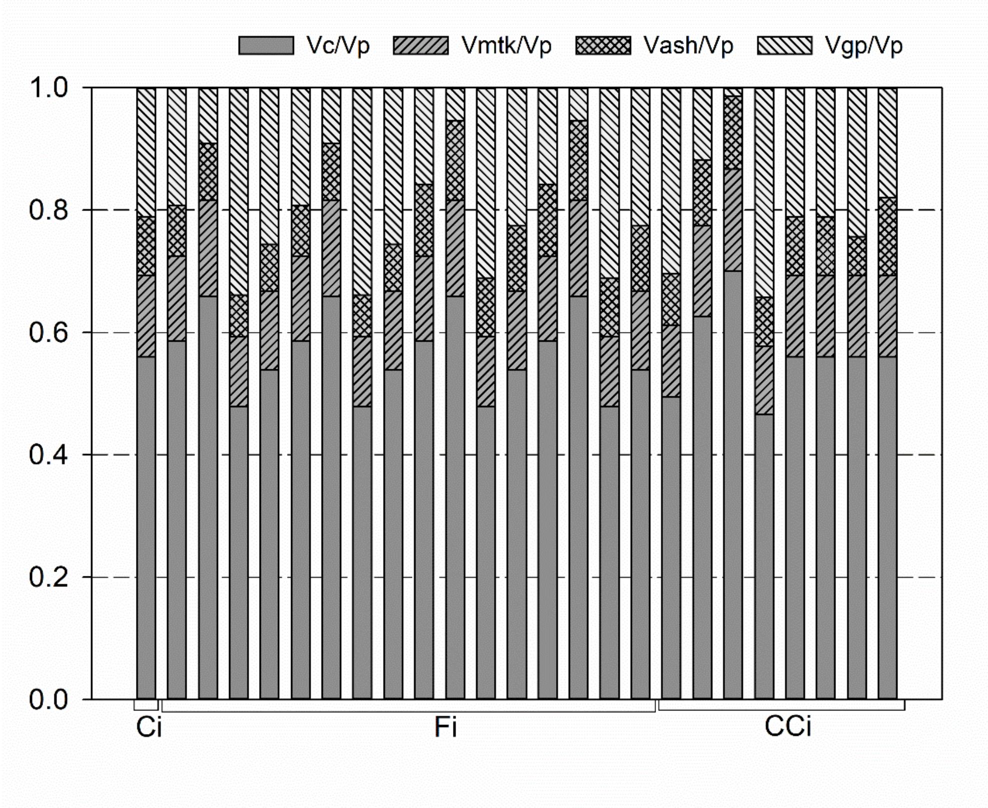

Fig. 4. Volume fraction of each material in powder mixtures

2.3 Material efficiency (ME) indicator

Nowadays, in the concrete mix-design process, the selection of materials has to meet environmental benefits in addition to the economic, safety, serviceability and durability requirements. One of the most often referred aspect of environmental impact of concrete structures is carbon footprint. According to ISO 14067 (ISO, 2018) "it is a sum of greenhouse gases emissions and removals in a product system expressed as CO_2 equivalent". In this work, concerning the environmental impact, the emphasis is placed on the global warming potential (GWP) of tested mixtures on volumetric basis.

Once the CCD plan mixtures were tested for their workability, mechanical performance and durability, the global warming potential (GWP) and unit cost were computed. The GWP of the tested mortars was estimated by multiplying the content of each constituent material in one m^3 of mortar by the respective CO_2 emissions per kg of material (provided in Table 6). According to the criteria defined in the European Union directive (EU, 2008), the biomass ash and granite powder were considered as wastes and thus no GWP allocation was performed. The unit cost of each mortar mixture was computed based on the individual costs of the constituent materials indicated in Table 6.

Table 6. GWP and cost considered for each constituent material

Material	GWP ($Kg\ CO_2/kg$)	Cost (€/kg)
Cement	0.830 (Chiaia et al., 2014)	0.100
Metakaolin	0.09240 (Müller et al., 2014)	0.425
Biomass ash	0	0
Granite powder	0	0
Sand	0.00246 (Chiaia et al., 2014)	0.01
Water	0.000318 (Abdollahnejad et al., 2017)	0
Superplasticizer	0.994 (Müller et al., 2014)	0.98

The ME indicator proposed herein is similar to the one proposed by Zhong et al. for ultra-high performance concrete (Zhong et al., 2018), and aims to reflect the material performance in terms of engineering properties (including workability, compressive strength, and a durability indicator) over its economic (unit cost) and environmental impact (GWP). Thus, in the current study, to quantify the ME, a dimensionless parameter was defined as follows (Eq. 2):

$$\mathrm{ME} = \frac{\mathrm{w1}\cdot\frac{\mathrm{Dflow}}{\mathrm{Dflow,ref}} + \mathrm{w2}\cdot\frac{\mathrm{fcm}}{\mathrm{fcm,ref}} + \mathrm{w3}\cdot\frac{\mathrm{Resis}}{\mathrm{Resis,ref}}}{\frac{\mathrm{GWP}}{\mathrm{GWP,ref}}\cdot\frac{\mathrm{Cost}}{\mathrm{Cost,ref}}}, \quad \textbf{Eq. 2}$$

where Dflow, fcm, Resis, GWP, and Cost represent the spread flow diameter, compressive strength, resistivity, GWP, and unit cost, respectively, of a given mortar mixture. Different importance can be assigned to each engineering property using the partial weights (wi), where ∑wi = 1.0. Dflow,ref; fcm,ref; Resis,ref; GWP,ref; and Cost,ref correspond to the values of a reference mixture or target values established in view of a given practical application.

The proposed indicator ME increases with the improvement of the material performance (increased spread flow, compressive strength, and/or resistivity) and is inversely proportional to the economic and environmental impact ratios such that lower cost and CO_2 allocation indicate a greater ME.

2.4 Test methods

All mortar mixes were prepared in 1.6 l batches and mixed in a mixer in accordance to EN 196-1 (AENOR, 2005). The batching sequence is displayed in Fig. 5. The mixer was set at a low constant speed ($140 \pm 5\ min^{-1}$).

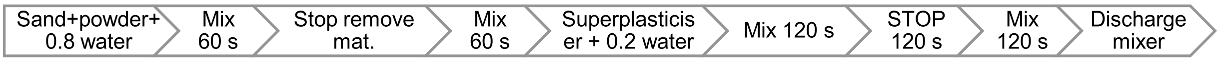

Fig. 5. Mixing procedure

Immediately after mixing, the mini-slump and mini-funnel tests, proposed by Okamura and Ouchi (Okamura and Ouchi, 2003), were performed to characterise the fresh state behaviour. For each mixture, five prismatic (40 x 40 x 160 mm^3) and three cylindrical (5 cm diameter and 3 cm height) specimens were cast to evaluate resistivity, compressive strength, porosity accessible to water, and resistance to carbonation. The specimens were stored in moulds for 24 h and subsequently cured under water at constant temperature of 20 ± 2 ºC until the testing age.

The cylindrical specimens were used to assess the porosity accessible to water at 28 days, according to the procedure described in (Moretti et al., 2018). The four prismatic specimens were used to assess the development of the electrical resistivity over time, which provides an indication of the microstructure development and pore connectivity. The measurements were performed at 28, 56, 110, and 147 days using the procedure described by Nunes et al. (Nunes and Costa, 2017). The two-electrode technique was used to measure the mortar's resistivity, using two stainless steel networks embedded at the ends of the prismatic specimens. The compressive strength was measured after a three-point bending test in two prismatic specimens, providing a mean value of four compressive strength results at both 28 and 147 days, and following standard EN 196-1 (AENOR, 2005).

Finally, one prismatic specimen was used to evaluate the resistance to carbonation (LNEC 391, 2004). The specimen was subjected to wet curing for 28 days, and was then stored in a room where the temperature and relative humidity was controlled for 14 days (20 ± 0.3 ºC and 50 ± 3%, respectively). Then, the specimen was exposed to 5 ± 0.1% CO_2 in an accelerated carbonation chamber (RH=60 ± 5%; Temp.= 23 ± 3 ºC). The carbonation depth was evaluated (using a phenolphthalein pH indicator) after approximately 180 days of exposure in the carbonation chamber. At the testing age, a thin slice was cut and the phenolphthalein was applied on the inner side.

The current experimental plan led to the collection of data on the following response variables: spread diameter (Dflow); time to flow through the funnel (Tfunnel), compressive strength (fcm_28d), resistivity (Resist_28d and Resist_56d), porosity accessible to water (Por_28d), and carbonation depth after six months of exposure inside the carbonation chamber (Carb_6m).

3 RESULTS

Table 7 displays the measured results of the different tested properties and Table 8 presents the corresponding statistical summary for the 28 experimental results and the four central mixtures. The results obtained for the four central mixtures provide information about the repeatability of the data. In the case of the CC1 mixture, flow time is not indicated because of the occurrence of blocking near the V-funnel exit. Consequently, a large value of 10000 was considered as the Tfunnel result for CC1 mixture.

Table 7. Results for all mixes in CCD plan

Ref	Dflow (mm)	Tfunnel (s)	fcm_28d (MPa)	Resist_28d (Ohm m)	Por_28d (%)	Carb_6m (mm)	ME
C1	318.8	17.5	71.9	143.3	18.1	4.0	1.04
C2	315.8	23.6	72.2	126.7	18.4	2.3	0.99
C3	326.0	20.1	69.9	129.4	18.1	5.5	1.00
C4	313.0	21.2	70.4	123.3	18.4	3.8	0.97
F1	219.8	43.2	73.9	189.0	17.2	0.0	0.93
F2	343.3	12.7	79.1	151.0	16.8	3.0	0.88
F3	207.5	61.8	65.0	120.5	17.4	4.0	1.04
F4	327.8	16.5	64.0	112.0	18.8	7.3	1.05
F5	258.5	33.5	75.3	187.2	17.2	2.5	0.96
F6	336.0	12.9	78.3	148.4	17.7	5.0	0.86
F7	260.5	39.2	64.9	106.3	17.8	4.8	1.05
F8	339.8	13.1	66.0	102.0	17.7	7.0	1.03
F9	231.5	45.8	77.6	170.0	17.2	0.0	0.92
F10	333.5	12.8	76.8	145.4	17.6	3.0	0.86
F11	226.5	51.2	63.3	104.0	18.4	4.4	1.00
F12	333.5	14.2	64.7	101.3	18.6	8.0	1.03
F13	281.8	31.8	75.5	181.6	17.4	2.0	0.97
F14	329.3	14.2	75.4	165.1	16.6	0.0	0.88
F15	278.5	37.0	64.4	109.5	18.4	5.8	1.08
F16	332.3	15.3	66.0	103.6	18.4	7.3	1.03
CC1	184.5	10000 (*)	68.5	146.3	16.5	3.5	0.99
CC2	364.0	9.2	68.1	123.9	17.3	0.0	0.92
CC3	310.0	23.1	87.4	219.3	16.9	0.0	0.87
CC4	301.0	22.5	58.4	82.8	19.4	11.8	1.10
CC5	305.5	19.2	71.9	130.3	17.9	2.5	1.00

CC6	332.5	18.8	71.5	135.2	18.0	3.8	1.02
CC7	319.5	23.7	69.7	124.6	15.8	4.0	0.98
CC8	330.8	18.3	72.4	132.6	15.6	4.3	1.02

*No measurement made owing to blocking of mortar at exit opening of the V-funnel

Table 8. Statistical parameters for all mixes and for central mix results

	Dflow (mm)	T funnel (s)	fcm,28d (MPa)	Resis 28d (ohm)	Por_28 (%)	Carb 6m (mm)	ME
All 28 mixtures							
Maximum	364.00	61.83	87.36	219.30	19.41	11.8	1.10
Minimum	184.50	9.25	58.42	82.80	15.64	0.00	0.86
Mean	298.61	24.90	70.82	136.24	17.65	3.91	0.982
Standard deviation	47.21	13.48	6.15	31.83	0.85	2.78	0.07
Coeff of variation (%)	16%	54%	9%	23%	5%	71%	7%
4 Central mixtures							
Maximum	326.00	23.60	72.19	143.27	18.45	5.50	1.04
Minimum	313.00	17.49	69.93	123.29	18.05	2.25	0.97
Mean	318.38	20.59	71.10	130.68	18.26	3.88	1.00
Standard deviation	5.60	2.53	1.12	8.76	0.19	1.33	0.03
Coeff. of variation (%)	2%	12%	2%	7%	1%	34%	3%

The current CCD plan allowed to obtain a wide range of mortar properties with: Dflow ranging from from 185 to 364 mm; Tfunnel ranging from 9.2 to 61.8 s; fcm_28d ranging from 58 to 87 MPa; Por_28d ranging from 16% to 19%; and Carb_6m ranging from 0 to 12 mm (see Table 8). In all cases, except for the Carb_6m, the coefficient of variation obtained with the total points was greater than the one achieved with only the central points (considered as the experimental error). This is an important premise to get a suitable model.

Fig. 6(a) displays the fresh test results, namely the V-funnel flow time as a function of the spread flow diameter. These results indicate that mortars exhibit relatively high funnel flow times, even for high spread diameters. Comparing the results with those of the literature (Fig. 6(b)), where the authors worked with binary/ternary binders that incorporated biomass ash

(Moretti et al., 2018), glass powder (Nunes et al., 2013), and spent equilibrium catalyst (Nunes and Costa, 2017), it can be observed that the funnel flow times are greater and spread diameters are in the same range. This effect is likely due to the wide variety of powder materials used in the current work, as they present a wide range of dimensions. It is relevant to mention that in all these studies (Moretti et al., 2018; Nunes et al., 2013; Nunes and Costa, 2017), the same type of fine aggregate (standard sand) and fine aggregate content were used (Vs/Vm = 0.475). Compared to other mixtures, the quaternary binder mixtures proposed in this study have the potential to lead to SCC mixtures with improved self-compacting ability, exhibiting higher deformability without compromising the mixtures stability (that is dependent on the paste phase viscosity).

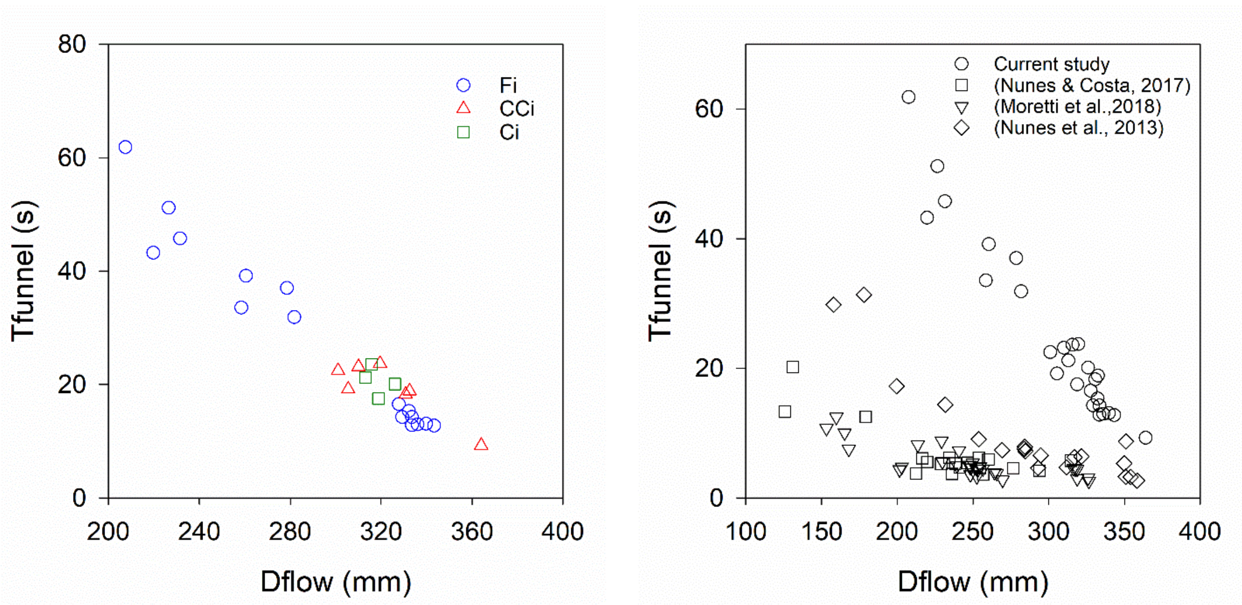

(a) (b)

Fig. 6. Range of fresh state results: (a) current study; (b) comparison with previous studies

Regarding the mechanical performance, Fig. 7 displays the compressive strength results at 28 and 147 days. The results of the compressive strength at 28 days (Fig. 7(a)) varied between 58 and 87 MPa, being greater than the results obtained by Destefani et al. (Destefani et al., 2016) and Moretti et al. (Moretti et al., 2018) for the same range of w/c ratio, as displayed in Fig. 7(b). At 147 days, the values are between 65 and 92 MPa, which implies an increase of between 6% and 19% compared to those obtained at 28 days, which can be explained by the pozzolanic activity of the metakaolin.

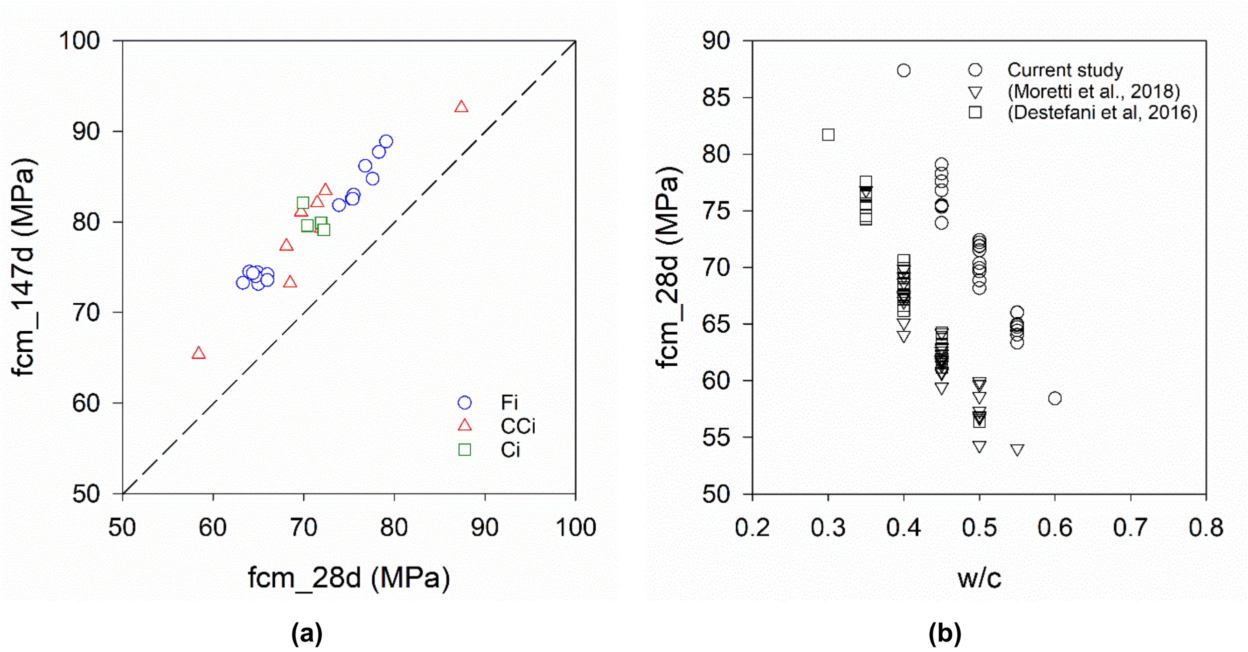

Fig. 7. Compressive strength results: (a) evolution from 28 to 147 days in current study; (b) comparison with previous studies results at 28 days

Fig. 8 displays the resistivity results at 56, 110, and 147 days compared to the resistivity measured at 28 days. From this graph, it can be concluded that from 28 to 147 days of age, there is a significant increase in resistivity (44%–88%), which reflects a progressive refinement of the microstructure with age, due to the pozzolanic activity of the metakaolin.

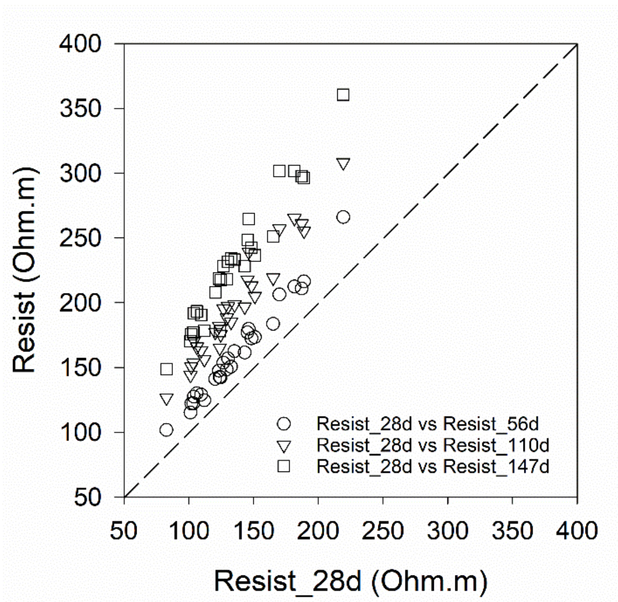

Fig. 8. Resistivity evolution in time

It is well known that a strong relationship between the electrical resistivity and durability exists. Resistivity indicates the ability to transport an electrical charge in a porous medium such as concrete, assuming that aggregates are electrically inert because their resistivity is several orders of magnitude greater than the pore solution. It is common knowledge that concrete electrical resistivity is mainly influenced by the w/c ratio, volume and type of cement, temperature and moisture conditions. Fig. 9(a) and Fig. 9(b) display the relationship between porosity and resistivity, and between resistivity and compressive strength at 28 days, respectively. It can be observed that there is a general tendency for increased resistivity when compressive strength is greater. Nevertheless, certain mixtures exhibit distinct resistivity values (and potentially different durability) for the same compressive strength level. In the same regard, in general, greater porosity values lead to reduced resistivity values.

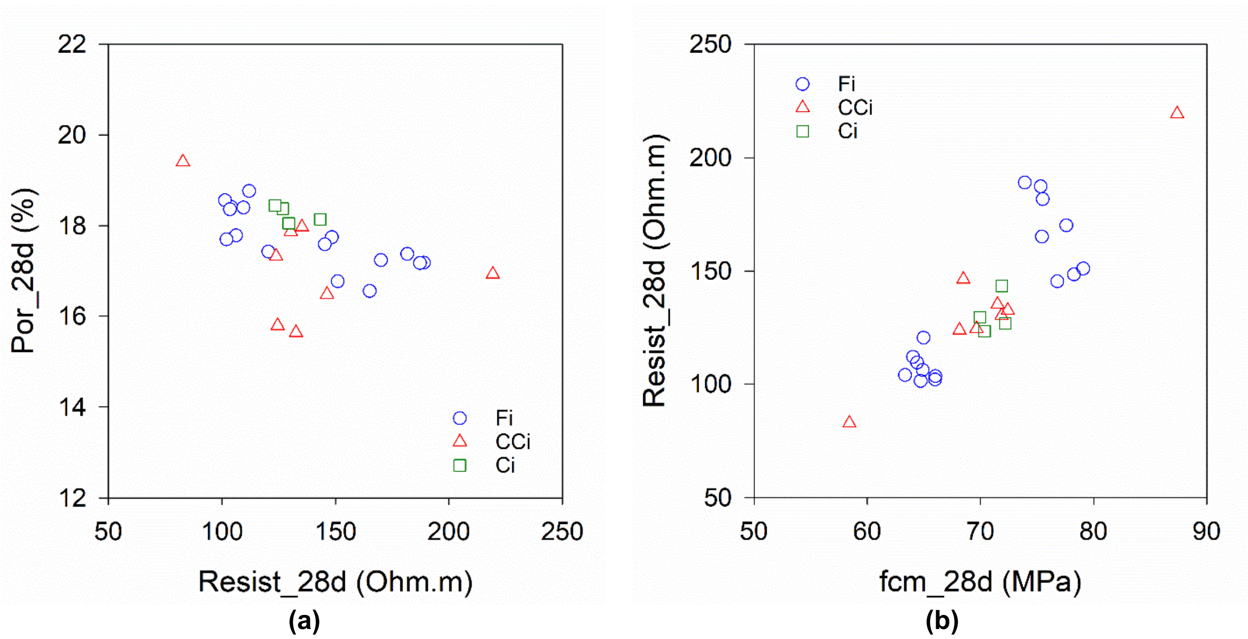

Fig. 9. (a) Resistivity versus porosity results at 28 days; (b) resistivity versus compressive strength results at 28 days

The last column of Table 7 presents the ME results calculated using Eq. 2. In the current study, the mixture corresponding to the central point in the CCD plan was considered the reference mixture. Thus, the average of the test results obtained with the four central mixes (see Table 8) was adopted as the reference value, namely Dflow,ref = 318 mm; fcm_28d,ref = 71 MPa; and Resis_28d,ref = 131 Ohm.m. The GWP and unit cost of the Ci mixture was computed as described in Section 2.3, leading to GWP,ref = 424 Kg CO_2/Kg and Cost,ref = 114 €/m^3. In this study, equal importance was attributed to the workability, mechanical strength, and durability, thus *wi* was defined as 33.3%.

4 ANALYSIS

4.1 Models identification

The CCD allows for building a second-order polynomial model providing information on the effect of independent variables and the variable interactions on the selected responses within previously defined limits of the experimental region. The general form of the second-order model and complete information about model identification process is clearly explained by Montgomery (Montgomery, 2012)

Numerical models were fitted using multilinear regression analysis based on the results shown in Table 7. An analysis of variance (ANOVA) was performed to validate the significance of the regression models and their regression coefficients. Fisher test and Student's test were developed to detect the non-significant variables. Then these variables were removed from the models. The significance level established to consider a variable in the model was 0.05. The estimation of the model parameters is based on the assumption that the errors are independent random variables with a mean of zero and constant variance. Tests of the hypotheses and interval estimation required the normality assumption of the errors. Several residuals analyses were conducted to verify the validity of these assumptions. To improve the statistical analysis the Cox-Box method was employed to determine a suitable power-based transformation (Montgomery, 2012). A comprehensive explanation of all the steps involved in the model identification and adequacy validation is provided by Montgomery (Montgomery, 2012) and previous publications by the authors (Matos et al., 2018; Nunes and Costa, 2017).

The fitted models for each measured response are provided in Table 9. The selected power-based transformation, correlation coefficients, parameter estimates, and standard deviation of the error term (the corresponding average is zero) are displayed in Table 7. The models are valid only within the defined boundaries of the experimental region, i.e., in the ranges between -2 and +2 of each factor (see Table 4).

Table 9. Fitted models (actual values of independent variables)

	ε, std.dev.	R^2/R^2adj
$Dflow = -12245.407 + 18197.271 \cdot \frac{Vw}{Vp} + 2036.667 \cdot \frac{w}{c} + 434447.917 \frac{Sp}{p} + 3962.708 \cdot \frac{ash}{c} - 486875.000 \cdot \frac{Vw}{Vp} \cdot \frac{Sp}{p} - 4512.500 \cdot \frac{Vw}{Vp} \cdot \frac{ash}{c} - 5199.375 \cdot \left(\frac{Vw}{Vp}\right)^2 - 2074.375 \cdot \left(\frac{w}{c}\right)^2$	8.549	0.967/0.953
$\frac{1}{T\ funnel} = -0.375 + 0.499 \cdot \frac{Vw}{Vp}$	5.72×10^{-3}	0.944/0.942

$\frac{1}{\sqrt{fcm\_28d}} = 0.248 - 0.423 \cdot \frac{Vw}{Vp} + 0.106 \cdot \frac{w}{c} + 0.245 \cdot \left(\frac{Vw}{Vp}\right)^2$	9.88×10^{-4}	0.963/0.958
$Resist_{28d} = 2884.307 - 1360.126 \cdot \frac{Vw}{Vp} - 4656.914 \cdot \frac{Sp}{p} - 5437.392 \cdot \frac{ash}{c} + 2413.597 \cdot \frac{Vw}{Vp} \cdot \frac{w}{c} + 337782.703 \cdot \frac{Sp}{p} \cdot \frac{ash}{c} + 1979.140 \cdot \left(\frac{w}{c}\right)^2 \cdot$	5.570	0.969/0.959
$Por_{28d} = -61.475 + 124.824 \frac{Vw}{Vp} + 10.600 \frac{w}{c} + 277.074 \frac{ash}{c} - 72.820 \left(\frac{Vw}{Vp}\right)^2 - 914.482 \left(\frac{ash}{c}\right)^2$	0.371	0.810/0.767
$Carb_{6m} = 43.374 - 207.226 \cdot \frac{w}{c} + 254.405 \cdot \left(\frac{w}{c}\right)^2$	1.537	0.694/0.670

The majority of the models exhibited high correlation coefficients (both R^2 and R^2adj > 0.90), which indicates that a significant proportion of the variability of the response variables is explained by the fitted models. The model fit to the Por_28d data exhibits an R^2 = 0.81, which could raise doubts regarding its accuracy; this is discussed further in the next section. In the case of Carb_6m, low correlation coefficients were obtained (R^2 = 0.69 and R^2adj = 0.67); thus, it was decided not to use this model for predictions.

4.2 Accuracy of fitted models

The suitability of fitted models was checked by comparing the predicted-to-measured values found with eight verification mortar mixes (see data in Table 10) not employed to derive the models. In these mixtures, the values of the mixture parameters fit within the boundaries of the experimental region. The predicted/measured ratio values for Dflow, Tfunnel, fcm_28d, Resis_28d, and Por_28d ranged between 0.98 and 1.06, 0.79 and 1.14, 0.93 and 1.02, 0.96 and 1.08, and 0.86 and 1.04, respectively. These results indicate acceptable accuracy of the derived statistical models. Moreover, it can be observed that in all cases, the measured values were within or near to upper and lower limits of the prediction intervals (see 95% PI Low and 95% PI High values in Table 10). Thus, it can be expected that the proposed models including the Por_28d model are sufficiently accurate to predict the tested mortar properties.

Table 10. Predicted vs. measured test results of eight verification mixes

			D flow (mm)	T funnel (s)	fcm_28d (MPa)	Resis_28d (Ohm)	Por_28d (%)
V1		Measured	317.25	18.99	70.32	122.74	18.15
Vw/Vp	0.85	Predicted	314.19	20.49	71.04	131.99	18.29
w/c	0.5	95% PI Low	291.82	16.39	68.44	118.08	17.40
Sp/p	0.016	95% PI High	336.56	27.32	73.79	145.91	19.19
ash/c	0.15	Pred/Meas	0.99	1.08	1.01	1.08	1.01
V2		Measured	315.75	20.31	70.12	128.85	17.74
Vw/Vp	0.85	Predicted	314.19	20.49	71.04	131.99	18.29
w/c	0.5	95% PI Low	291.82	16.39	68.44	118.08	17.40
Sp/p	0.016	95% PI High	336.56	27.32	73.79	145.91	19.19
ash/c	0.15	Pred/Meas	0.995	1.009	1.013	1.024	1.031
V3		Measured	315.25	23.16	74.89	137.27	18.20
Vw/Vp	0.85	Predicted	314.19	20.49	71.04	131.99	18.29
w/c	0.5	95% PI Low	291.82	16.39	68.44	118.08	14.70
Sp/p	0.016	95% PI High	336.56	27.32	73.79	145.91	19.19
ash/c	0.15	Pred/Meas	1.00	0.88	0.95	0.96	1.00
V4		Measured	308.5	21.31	71.57	--	17.63
Vw/Vp	0.85	Predicted	303.89	20.49	71.04	131.14	18.29
w/c	0.5	95% PI Low	281.09	16.39	68.44	116.95	17.40
Sp/p	0.0155	95% PI High	326.68	27.32	73.79	145.32	19.19
ash/c	0.15	Pred/Meas	0.99	0.96	0.99	--	1.04
V5		Measured	325.50	17.10	63.62	--	18.13
Vw/Vp	0.9	Predicted	344.90	13.56	64.82	111.56	18.05
w/c	0.55	95% PI Low	317.56	11.60	62.49	94.26	17.13
Sp/p	0.015	95% PI High	372.23	16.31	62.49	128.85	18.97
ash/c	0.125	Pred/Meas	1.06	0.79	1.02	--	1.00
V6		Measured	165.75	*	72.51	134.72	17.23
Vw/Vp	0.75	Predicted	173.05		67.47	147.32	17.46
w/c	0.5	95% PI Low	146.35		64.57	132.36	16.40
Sp/p	0.016	95% PI High	199.75		70.57	162.29	18.53
ash/c	0.15	Pred/Meas	1.04	--	0.93	1.09	1.01
V7		Measured	290.25	24.85	72.70	135.91	18.38
Vw/Vp	0.85	Predicted	307.83	20.49	71.04	133.63	15.87
w/c	0.5	95% PI Low	283.83	16.39	68.44	118.67	14.80

Sp/p	0.016	95% PI High	331.84	27.32	73.79	148.60	16.94
ash/c	0.1	Pred/Meas	1.06	0.82	0.98	0.98	0.86
V8		Measured	325.75	17.95	71.33	123.74	18.28
Vw/Vp	0.85	Predicted	320.54	20.49	71.04	130.35	16.14
w/c	0.5	95% PI Low	296.54	16.39	68.44	115.38	15.08
Sp/p	0.016	95% PI High	344.55	27.32	73.79	145.31	17.21
ash/c	0.2	Pred/Meas	0.984	1.142	0.996	1.053	0.883

*No measurement made owing to blocking of mortar at the exit opening of the V-funnel

4.3 Most significant effects

The fitted models expressed in terms of coded values allow for the analysis of the relative influence of the linear, interaction, and quadratic effects of the independent variables on each response variable. That is, the adjusted tuning parameters provide indication measure of the relative influence of each model term on the response variable, as represented in Fig. 10.

Analysing Fig. 10, it is clear that the most important variables affecting the mortar properties are Vw/Vp and w/c. The first significantly influences the fresh mortar properties; whereas the second influences notably the hardened mortar properties. In addition to the significant first order effects illustrated in Fig. 10, interaction effects between the variables and quadratic effects were also identified as significant. The most relevant of these was a quadratic effect of ash/c on the porosity accessible to water.

In this study the amount of metakaolin depends directly on the amount of cement, i.e., when the amount of cement increases, the amount of metakaolin also increases, because the mk/c ratio was fixed (mk/c = 20%). Therefore, the significant effect of the w/c variable actually translates into the significant effect of the water/binder variable, the binder being constituted by the cement plus metakaolin.

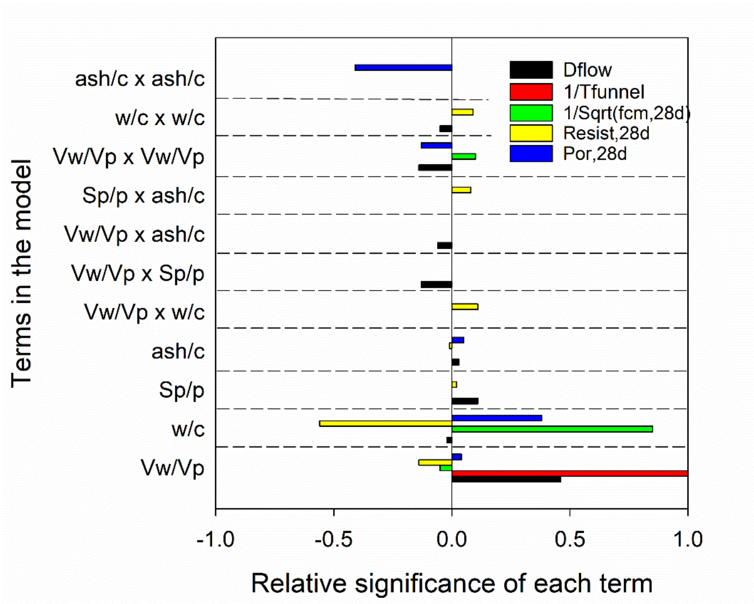

Fig. 10. Relative significance of each term in model for different response variables

In the current study, the content of the granite powder in the mortar mixtures was dependent on w/c, Vw/Vp, and ash/c. The granite powder volume fraction in powders (Vgp/Vp) can be computed as follows:

$$V_{GP}/V_P = 1 - \frac{Vw/Vp}{w/c} \cdot \left(1/\rho_C + \frac{0{,}2}{\rho_{mk}} + \frac{ash/c}{\rho_{BA}}\right) \cdot \rho_W, \qquad \textbf{Eq. 3}$$

where ρ_c, ρ_{mk}, ρ_{BA}, and ρ_w are the specific density of cement, metakaolin, bottom ash, and water, respectively. Fig. 11 represents this relation graphically to facilitate the interpretation of the effect of w/c and Vw/Vp on the GP volume fraction in the powder mixtures. Eq. 3 reveals that Vgp/Vp decreases by increasing Vw/Vp or by increasing ash/c, while maintaining w/c constant. Conversely, when w/c increases and the remaining variables are held constant, Vgp/Vp increases.

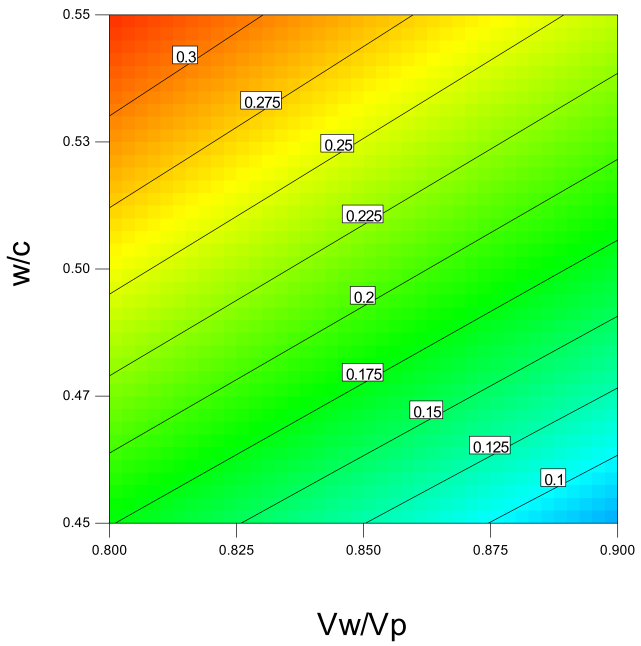

Fig. 11. Contour plot of GP volume fraction (%) in powder mixtures while maintaining ash/c = 0.15

In Fig. 12, the ME indicator, computed using Eq. 2 and the estimated properties at 28 days (using the numerical models presented in Table 9), is plotted by changing only one design variable over its range while holding all other design variables constant. This plot facilitates the comparison of the effects of all the design variables on the ME. The steep slope in w/c and curvature in Vw/Vp indicate that the ME is sensitive to these factors. Conversely, the ME indicates insensitivity to changes in Sp/p and ash/c, which can be explained by the relatively limited range of variation of these two variables in this study. Clearly, the w/c level is the most influencing parameter on the final ME value.

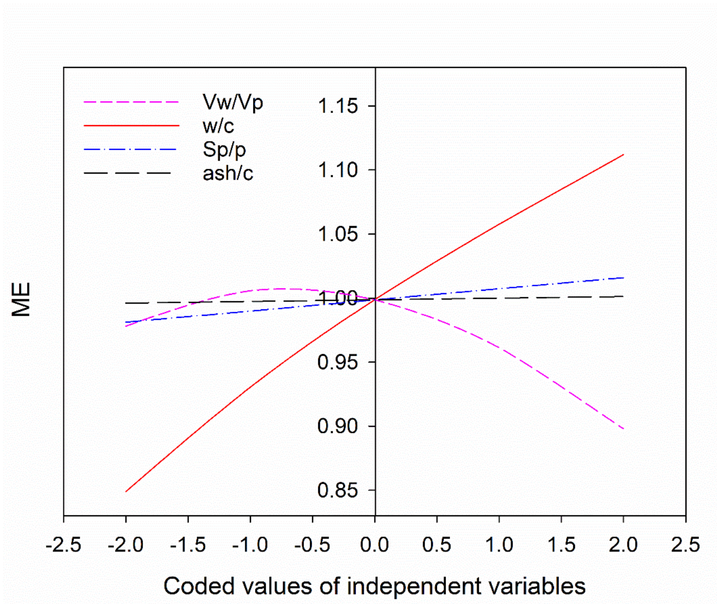

Fig. 12. Influence of each design variable on ME

4.4 Mixtures optimisation

To optimise the mortar properties, first, the Tfunnel model was analysed, which depends only on Vw/Vp. A minimum value of Vw/Vp is of interest to increase VGP/Vp (according to Eq. 3); however, Fig. 13(a) indicates that at less than a certain level of Vw/Vp, the V-funnel flow time increases drastically, accompanied by an increase in the variation of the results. Considering this, a target Tfunnel of 25 s was established and Vw/Vp was derived using the Tfunnel model and set equal to 0.832 (see Fig. 13(a)). After fixing the Vw/Vp level, the compressive strength at 28 days became dependent on the w/c level only, as indicated in Fig. 13(b). Therefore, using the fcm_28 model (Table 9), the w/c ratio was set to allow achieving four different levels of compressive strength at 28 days, namely 65, 70, 75, and 80 MPa, as indicated in Fig. 13(b). Finally, the remaining design variables (ash/c and Sp/p) were established to obtain a Dflow in the range [300, 320] (mm) and, simultaneously, maximise the ME.

The graphical optimisation module in Design-Expert software was used to find the region where the acceptable response outcomes could be found. For this purpose, the ME_28d response was simulated via Eq. 2 and supplied to Design-Expert. The four selected optimal solutions are presented in Table 11 in terms of the coded values. After finding the candidate optimal solutions, the distance to the centre of the CCD plan (*d*) should be computed as follows:

$$d = \sqrt{\sum_{i=1}^{4} Xi^2}, \qquad \textbf{Eq. 4}$$

where X_i refers to the design variables value in terms of the coded values. The distance to the centre of the CCD plan should not exceed "2" by any considerable amount, because the fitted models could possibly no longer predict, in a reasonable manner, outside of the CCD region. The distance to the centre of the CCD for each optimised mixture is presented in Table 11; this was not excessive.

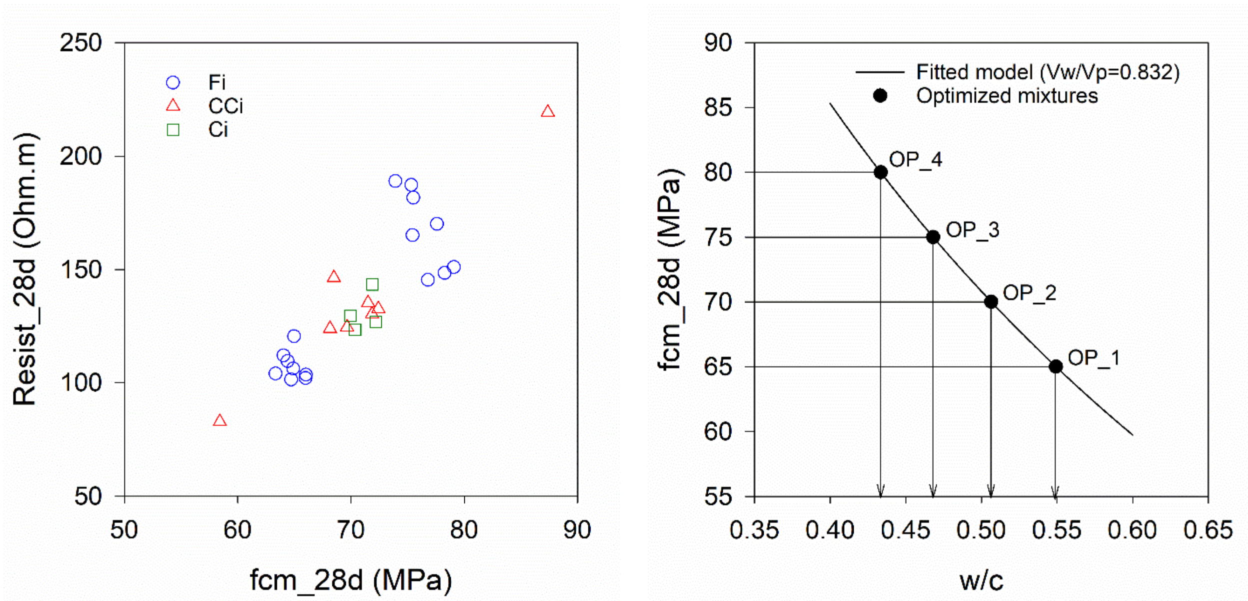

(a) **(b)**

Fig. 13. Selection of (a) Vw/Vp level and (b) the four selected levels of w/c

The four optimised mortar mixtures were also prepared and tested in the lab using the same mixing protocol and test procedures described in Section 2.2. Table 11 provides the corresponding experimental test results with the predicted response values and prediction intervals. The comparison between the predicted and experimental results obtained (all within the 95% prediction interval) again confirms the accuracy of the fitted models. The average carbonation depth, after 242 days of exposure in the carbonation chamber, is also reported in Table 7 and can be observed in Fig. 14.

Table 11. Optimised mixtures and corresponding predicted and measured test results

Ref.		d		Dflow (mm)	T funnel (s)	fcm_28d (MPa)	Resist_28d	Por_28d	Carb_242d (mm)
OP_1		2.36	Measured	320.25	22.99	66.28	110.68	17.46	6.0
Vw/Vp	-0.353		Predicted	319.25	25.00	64.99	115.99	17.55	

w/c	0.986		95% PI Low	294.72	19.14	62.68	98.97	16.59	
Sp/p	1.468		95% PI High	343.78	36.01	67.44	133.01	18.51	
ash/c	1.525		Pred/Meas	1.00	1.09	0.98	1.05	1.01	
OP_2			Measured	315.75	22.32	71.02	141.15	17.89	3.5
Vw/Vp	-0.353		Predicted	319.52	25.00	70.00	130.94	18.30	
w/c	0.131	1.68	95% PI Low	295.89	19.14	67.46	116.26	17.41	
Sp/p	1.627		95% PI High	343.16	36.01	72.68	145.61	19.19	
ash/c	-0.141		Pred/Meas	1.01	1.12	0.99	0.93	1.02	
OP_3			Measured	311.25	29.61	76.47	171.25	17.74	1.5
Vw/Vp	-0.353		Predicted	319.32	25.00	75.00	161.77	17.82	
w/c	-0.637	1.68	95% PI Low	295.93	19.15	72.17	147.02	16.92	
Sp/p	1.429		95% PI High	342.71	36.01	78.01	176.52	18.71	
ash/c	0.488		Pred/Meas	1.02	0.84	0.98	0.94	1.00	
OP_4			Measured	317.67	27.63	81.43	193.16	17.31	1
Vw/Vp	-0.353		Predicted	312.40	25.00	79.99	193.97	16.06	
w/c	-1.331	2.36	95% PI Low	287.71	19.14	76.80	177.64	15.06	
Sp/p	0.930		95% PI High	337.08	36.01	83.39	210.30	17.05	
ash/c	1.676		Pred/Meas	0.98	0.90	0.98	1.00	0.93	

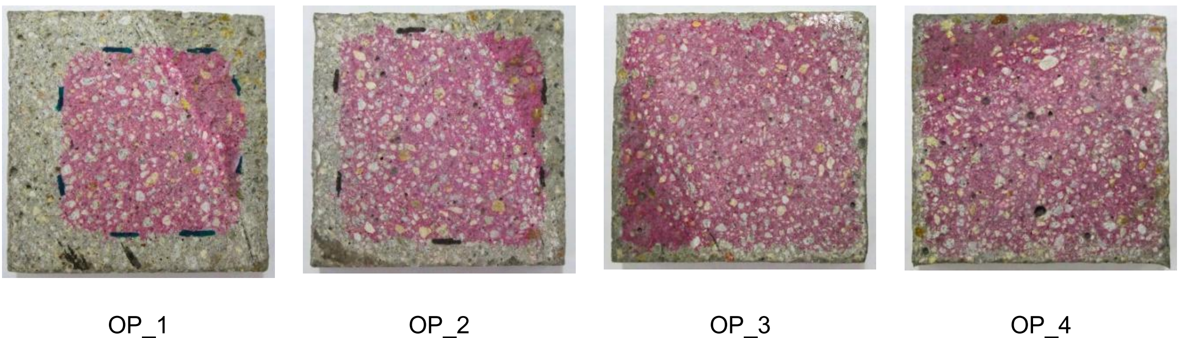

Fig. 14. Comparison of carbonation depth (whitish part) on optimised mortar specimens

Fig. 15 displays the powder composition of each of the optimal mixtures by volume. It clearly indicates that it is possible to incorporate significant amounts of granite powder and biomass ash in SCC while achieving excellent self-compacting ability. All optimal mortars exhibited a considerable spread flow diameter accompanied by a high flow time, which is important to guarantee stable mixtures. However, the optimised mixtures are distinct in terms of compressive strength, resistivity, and resistance to carbonation, as evidenced from the results of Table 7 and Fig. 6, Fig. 7, Fig. 8, and Fig. 9.

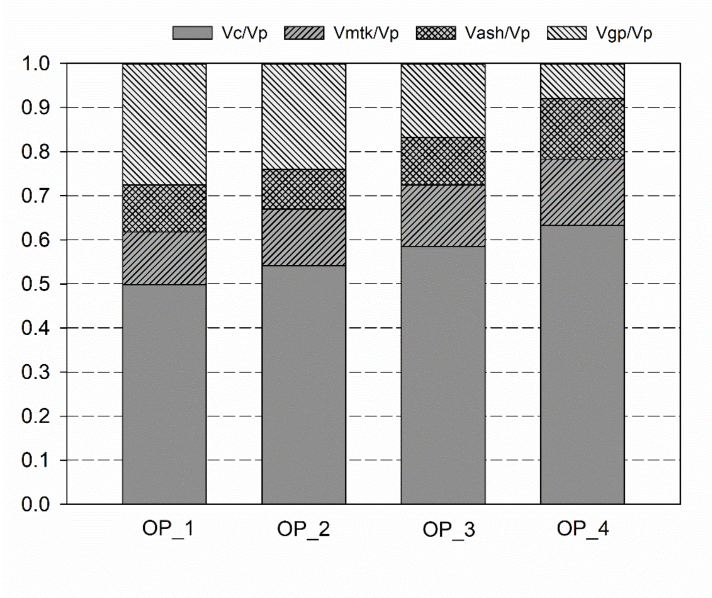

Fig. 15. Volume fraction of each material in powder mixtures for optimised mortars

Again, using the central mixture as a reference mixture, the ME was computed for all four optimised mixtures and is reported in Table 12. The results of individual ratios used in Eq. 2 to compute the ME are also presented in Table 12 to assess the relative influence of the engineering properties, and economic and environmental impacts on the ME. Because OP_2 and the central mixture exhibit similar properties, the resulting ME is near to 1.0. The replacement of the binder with wastes (that is a consequence of increasing the w/c ratio in our formulation) increased the ME. The reduced performance of OP_1 in terms of compressive strength and resistivity was outbalanced by the improved cost and environmental impacts, leading to a greater ME. The opposite occurs with mixture OP_3, and is even more pronounced with mixture OP_4.

Table 12. ME of optimised mixtures

Ref.	$\frac{\text{Dflow}}{\text{Dflow, ref}}$	$\frac{\text{fcm}}{\text{fcm, ref}}$	$\frac{\text{Resis}}{\text{Resis, ref}}$	$\frac{\text{GWP}}{\text{GWP, ref}}$	$\frac{\text{Cost}}{\text{Cost, ref}}$	ME
OP_1	1.00	0.91	0.89	0.91	0.93	1.11
OP_2	1.00	0.98	1.00	0.98	0.99	1.03
OP_3	0.99	1.05	1.21	1.06	1.05	0.98
OP_4	0.98	1.13	1.48	1.14	1.11	0.95

5 CONCLUSIONS

Based on the above-presented results and discussions, the following conclusions can be drawn:

- Statistically designed experiments (using a CCD plan) revealed that Vw/Vp had a greater effect on the fresh state properties whereas w/c was the most significant variable in terms of the analysed hardened state properties.
- Cement, metakaolin, biomass ash, and granite powder can be used together in quaternary blends allowing the production of cleaner SCC mortars with improved workability and relatively high viscosity.
- In terms of compressive strength (28 days), the quaternary blends tested in this study exhibited improved behaviour when compared to the results reported by other authors for the same w/c ratio range, equally fine aggregate content, and same type of fine aggregate.
- A material efficiency (ME) indicator was proposed to reflect the influence of the engineering properties (such as compressive strength, workability, and durability), unit cost, and GWP. The ME was found to be more sensitive to changes in w/c and Vw/Vp, w/c being the most influencing parameter on the final ME value.
- Four different mortar mixtures were optimised to achieve excellent self-compacting ability, yet with distinct compressive strength levels at 28 days (65, 70, 75, and 80 MPa), resistivity, and resistance to carbonation. Optimised paste mixtures could be used to produce SCCs (replacing the standard sand by real aggregates) with performance levels directly correlated to those of the mortars.

The results presented herein are promising for engineers, concrete producers and other construction sector agents willing to achieve both environmental and economic gains in the short term. This is particularly true in the "Galicia–North of Portugal Euroregion" where biomass ash and granite powder (both industrial wastes from local industry) are abundant.

It is important to emphasise that the proposed numerical models are valid for the selected set of materials, and substantial changes in the chemical composition and/or physical characteristics of the materials used would require validation of proposed models.

Acknowledgements

This work was financially supported by: Base Funding - UIDB/04708/2020 and Programmatic Funding - UIDP/04708/2020 of the CONSTRUCT - Instituto de I&D em Estruturas e Construções - funded by national funds through the FCT/MCTES (PIDDAC).; by the INBRAIL project - POCI-01-0247-FEDER-033990 funded by FEDER funds through COMPETE2020 - Programa Operacional Competitividade e Internacionalização (POCI) and Programa Operacional da Região de Lisboa within Sistema de Incentivos à Investigação e Desenvolvimento (SI IDT) from Portugal 2020 “Projetos I&DT Empresas em Co promoção”. The study is part of two projects entitled: “Robust self-compacting recycled concretes: rheology in fresh state and mechanical properties (Ref: BIA2014-58063-R)” and “Sustainable High Performance Self-Compacting Concrete using low clinker cement, and integral curing and self-healing agents (HACCURACEM) (BIA2017-85657-R)” funded by MINECO.

Moreover, this work was also made possible by the financial support of a pre-doctoral grant of MINECO (FPI 2015) and two grants for international pre-doctoral stays: (a) FPI 2015 and (b) IACOBUS program for “Galicia–North of Portugal Euroregion”.

References

Abdollahnejad, Z., Miraldo, S., Pacheco-Torgal, F., Aguiar, J.B., 2017. Cost-efficient one-part alkali-activated mortars with low global warming potential for floor heating systems applications. Eur. J. Environ. Civ. Eng. 21, 412–429. https://doi.org/10.1080/19648189.2015.1125392

AENOR, 2005. UNE -EN 196-1. Cement Test Methods. Part 1: Determination of Mechanical Resistances (in Spanish). Madrid, Spain.

AFNOR, 2012. NF P18-513, Additions for concrete — Metakaolin — Specifications and conformity criteria (in French).

Amaral, L.F., Girondi Delaqua, G.C., Nicolite, M., Marvila, M.T., de Azevedo, A.R.G., Alexandre, J., Fontes Vieira, C.M., Monteiro, S.N., 2020. Eco-friendly mortars with addition of ornamental stone waste - A mathematical model approach for granulometric optimization. J. Clean. Prod. 248, 119283. https://doi.org/10.1016/j.jclepro.2019.119283

Aprianti S, E., 2017. A huge number of artificial waste material can be supplementary cementitious material (SCM) for concrete production – a review part II. J. Clean. Prod. 142, 4178–4194. https://doi.org/10.1016/j.jclepro.2015.12.115

Cheah, C.B., Ramli, M., 2011. The implementation of wood waste ash as a partial cement replacement material in the production of structural grade concrete and mortar: An overview. Resour. Conserv. Recycl. 55, 669–685. https://doi.org/10.1016/j.resconrec.2011.02.002

Chiaia, B., Fantilli, A.P., Guerini, A., Volpatti, G., Zampini, D., 2014. Eco-mechanical index for structural concrete. Constr. Build. Mater. 67, 386–392. https://doi.org/10.1016/j.conbuildmat.2013.12.090

de Azevedo, A.R.G., Alexandre, J., Marvila, M.T., Xavier, G. de C., Monteiro, S.N., Pedroti, L.G., 2020. Technological and environmental comparative of the processing of primary sludge waste from paper industry for mortar. J. Clean. Prod. 249, 119336. https://doi.org/10.1016/j.jclepro.2019.119336

Destefani, A., Nunes, S., Sousa-Coutinho, J., 2016. Argamassa auto-compactável com pó de mármore em portugal, in: Encontro Nacional BETÃO ESTRUTURAL-BE2016 FCTUC. pp. 1–10.

Enersilva, 2007. Promotion of the use of forest biomass for energy purposes in south-west Europe (2004-2007) (in Spanish).

Esmaeilkhanian, B., Khayat, K.H., Wallevik, O.H., 2017. Mix design approach for low-powder self-consolidating concrete: Eco-SCC—content optimization and performance. Mater. Struct. 50, 124. https://doi.org/10.1617/s11527-017-0993-y

EU, 2008. Directive 2008/98/EC of the European Parliament and of the Council of 19 November 2008 on waste and repealing certain Directives, European Parliament.

Europeas, C. las C., 2000. Green Book: hacia una estrategia eurpea de seguridad del abastacemiento energético. Bruselas.

Eurorregión Galicia-Norte de Portugal (AECT) | POCTEP [WWW Document], n.d. URL https://poctep.eu/es/2014-2020/eurorregión-galicia-norte-de-portugal-aect (accessed 3.16.20).

Galetakis, M., Soultana, A., 2016. A review on the utilisation of quarry and ornamental stone industry fine by-products in the construction sector. Constr. Build. Mater. https://doi.org/10.1016/j.conbuildmat.2015.10.204

Gartner, E., Hirao, H., 2015. A review of alternative approaches to the reduction of CO 2 emissions associated with the manufacture of the binder phase in concrete. Cem. Concr. Res. 78, 126–142. https://doi.org/10.1016/j.cemconres.2015.04.012

González-Taboada, I., González-Fonteboa, B., Martínez-Abella, F., Carro-López, D., 2017. Self-compacting recycled concrete: Relationships between empirical and rheological parameters and proposal of a workability box. Constr. Build. Mater. 143, 537–546. https://doi.org/10.1016/j.conbuildmat.2017.03.156

ISO, 2018. ISO 14067:2018(en), Greenhouse gases — Carbon footprint of products — Requirements and guidelines for quantification [WWW Document]. URL https://www.iso.org/obp/ui#iso:std:iso:14067:ed-1:v1:en (accessed 3.17.20).

Khayat, K., De Schutter, G., 2014. Mechanical properties of self-compacting concrete : state-of-the-art report of the RILEM technical committee 228-MPS on mechanical properties of self-compacting concrete, RILEM State-of-the-Art Reports.

LNEC 391, 2004. Concrete: Determination of carbonation resistance (in Portuguese).

Matos, A.M., Maia, L., Nunes, S., Milheiro-Oliveira, P., 2018. Design of self-compacting high-performance concrete: Study of mortar phase. Constr. Build. Mater. 167, 617–630. https://doi.org/10.1016/j.conbuildmat.2018.02.053

Mo, K.H., Alengaram, U.J., Jumaat, M.Z., Yap, S.P., Lee, S.C., 2016. Green concrete partially comprised of farming waste residues: a review. J. Clean. Prod. 117, 122–138. https://doi.org/10.1016/j.jclepro.2016.01.022

Montani, C., 2017. Marble and Stones in the World XXVIII Report.

Montgomery, D.C., 2012. Design and Analysis of ExperimentsDOUGLAS C. MONTGOMER - Eighth Edition, Design. John Wiley and sons Inc., United States of America. https://doi.org/10.1198/tech.2006.s372

Moretti, J.P., Nunes, S., Sales, A., 2018. Self-compacting concrete incorporating sugarcane bagasse ash. Constr. Build. Mater. 172, 635–649. https://doi.org/10.1016/j.conbuildmat.2018.03.277

Müller, H.S., Haist, M., Vogel, M., 2014. Assessment of the sustainability potential of concrete and concrete structures considering their environmental impact, performance and lifetime. Constr. Build. Mater. 67, 321–337. https://doi.org/10.1016/j.conbuildmat.2014.01.039

Nunes, S., Costa, C., 2017. Numerical optimization of self-compacting mortar mixture containing spent equilibrium catalyst from oil refinery. J. Clean. Prod. 158, 109–121. https://doi.org/10.1016/j.jclepro.2017.04.161

Nunes, S., Matos, A.M., Duarte, T., Figueiras, H., Sousa-Coutinho, J., 2013. Mixture design of self-compacting glass mortar. Cem. Concr. Compos. 43, 1–11. https://doi.org/10.1016/j.cemconcomp.2013.05.009

Okamura, H., Ouchi, M., 2003. Self-Compacting Concrete. J. Adv. Concr. Technol. 1, 5–15.

Paris, J.M., Roessler, J.G., Ferraro, C.C., DeFord, H.D., Townsend, T.G., 2016. A review of waste products utilized as supplements to Portland cement in concrete. J. Clean. Prod. 121, 1–18. https://doi.org/10.1016/j.jclepro.2016.02.013

Pavlíková, M., Zemanová, L., Pokorný, J., Záleská, M., Jankovský, O., Lojka, M., Pavlík, Z., 2019. Influence of Wood-Based Biomass Ash Admixing on the Structural, Mechanical, Hygric, and Thermal Properties of Air Lime Mortars. Materials (Basel). 12, 2227. https://doi.org/10.3390/ma12142227

Scrivener, K.L., John, V.M., Gartner, E.M., 2018. Eco-efficient cements: Potential economically viable solutions for a low-CO 2 cement-based materials industry. Cem. Concr. Res. 114, 2–26. https://doi.org/10.1016/j.cemconres.2018.03.015

Scrivener, K.L., John, V.M., Gartner, E.M., 2016. Eco-efficient cements: Potential, economically viable solutions for a low-CO2, cement-based materials industry 114, 2–26.

Shi, C., Qu, B., Provis, J.L., 2019. Recent progress in low-carbon binders. Cem. Concr. Res. 122, 227–250. https://doi.org/10.1016/j.cemconres.2019.05.009

Swaminathen, A.N., 2013. Indian rice husk ash - Improving the strength and durability of concrete: A review, in: 2013 International Conference on Current Trends in Engineering and Technology, ICCTET 2013. IEEE, pp. 16–17. https://doi.org/10.1109/ICCTET.2013.6675903

Zhong, R., Wille, K., Viegas, R., 2018. Material efficiency in the design of UHPC paste from a life cycle point of view. Constr. Build. Mater. 160, 505–513. https://doi.org/10.1016/j.conbuildmat.2017.11.049